Available online at www.sciencedirect.com
ScienceDirect
Environmental Pollution 148 (2007) 842–854
ENVIRONMENTAL POLLUTION
www.elsevier.com/locate/envpol

Future climate scenarios and rainfall–runoff modelling in the Upper Gallego catchment (Spain)

C.M. Bürger [a,*], O. Kolditz [a], H.J. Fowler [b], S. Blenkinsop [b]

[a] GeoSystemsResearch, Center for Applied Geosciences, Sigwartstrasse 10, 72076 Tübingen, Germany
[b] School of Civil Engineering and Geosciences, Cassie Building, University of Newcastle upon Tyne, NE1 7RU, Germany

Received 5 February 2007; accepted 6 February 2007

Future climate change and data-based rainfall–runoff predictions are presented for the Upper Gallego.

Abstract

Global climate change may have large impacts on water supplies, drought or flood frequencies and magnitudes in local and regional hydrologic systems. Water authorities therefore rely on computer models for quantitative impact prediction. In this study we present kernel-based learning machine river flow models for the Upper Gallego catchment of the Ebro basin. Different learning machines were calibrated using daily gauge data. The models posed two major challenges: (1) estimation of the rainfall–runoff transfer function from the available time series is complicated by anthropogenic regulation and mountainous terrain and (2) the river flow model is weak when only climate data are used, but additional antecedent flow data seemed to lead to delayed peak flow estimation. These types of models, together with the presented downscaled climate scenarios, can be used for climate change impact assessment in the Gallego, which is important for the future management of the system.

Keywords: Climate change; Rainfall–runoff; Hydrology; Kernel-methods; Weather scenarios

1. Introduction

A major challenge still remaining in hydrology is the accurate prediction of catchment runoff responses to rainfall events. Quantitative descriptions of this dynamic transformation process are necessary for the optimal design of water storage and drainage networks or the management of extreme events, such as floods or droughts (e.g. Sivakumar et al., 2002). Computer models used for the calculation of runoff responses range from physically-based distributed models like 'Systeme Hydrologique Europeen' (SHE, Abbott et al., 1986) to conceptual more lumped models (e.g. TOPMODEL, Beven and Freer, 2001; TRANSEP, Weiler et al., 2003) to black-box models like artificial neural networks (ANN). The latter are data-driven and try to simulate the dependent variable runoff based on (measurable) input variables such as rainfall, temperature, or earlier runoff. No physical process description is used, however, its functional form is estimated based on the proper balance of model fit and model complexity (here we refer to the number of fitting parameters). ANN have been successfully applied to numerous rainfall–runoff problems among various catchments within the last decade (e.g. Minns and Hall, 1996; Shamseldin, 1997; Dawson and Wilby, 1999; Sajikumar and Thandaveswara, 1999; Zealand et al., 1999; Gautam et al., 2000; Tokar and Markus, 2000; Anctil et al., 2004; Rajurkar et al., 2004). Recent research has also tried to integrate ANN with conceptual models (e.g. Jain and Srinivasulu, 2004; Chen and Barry, 2006) or used data-based ANNs for flood prediction in ungauged catchments (Dawson et al., 2006).

This study, part of the integrated EU-Project AquaTerra (AT), focuses on data-based modelling and applies two relatively new types of 'kernel-based learning machines': support vector machines (SVM, Boser et al., 1992; Vapnik, 1998; Schölkopf and Smola, 2002) and relevance vector machines

* Corresponding author. Tel.: +49 (0) 7071 29 73179; fax: +49 (0) 7071 5059.
E-mail address: claudius.buerger@uni-tuebingen.de (C.M. Bürger).

0269-7491/$ - see front matter © 2007 Elsevier Ltd. All rights reserved.
doi:10.1016/j.envpol.2007.02.002

(RVM, Tipping, 2001). Recent applications of these learning machines in the field of hydrology and groundwater management include multi-time scale stream flow forecasting (Asefa et al., 2006), lake level phase–space reconstructions (Khalil et al., 2006), and the simulation of nitrate concentrations in groundwater at pre-defined receptors (Khalil et al., 2005). A first rainfall–runoff study with SVM can be found in Dibike et al. (2001). Some of these studies report very high, if not the best, predictive performances for SVM and RVM relative to other data-based models. Following this, we develop learning machine models to simulate the catchment response of the anthropogenically influenced Upper Gallego river in northern Spain, utilizing rainfall, temperature and reservoir lake volume data in order to make daily discharge forecasts at the gauging station Anzanigo.

Learning machine approaches have been little used within climate change impact studies, but may offer an alternative approach to the use of fully-distributed rainfall–runoff models for the prediction of future impacts on flow. Within Spain, significant increases in mean annual and seasonal temperatures have been observed over the 20th century (Esteban-Parra et al., 2003), with decreases in rainfall over the Iberian Peninsula observed since the early 1960s (Goodess and Jones, 2002; Palutikof, 2003), but increases over the northern coastal regions of Spain (Esteban-Parra et al., 2003). Changes in climate along the Mediterranean coast have received particular attention in the literature (De Luís et al., 2000; Ramos and Martínez-Casasnovas, 2006; Martínez et al., 2007) due to their potential impact on water resources in the region.

Within this study we present the projected changes in future precipitation and temperature for the Gallego catchment and larger Ebro river basin based on simulations from 11 Regional Climate Models (RCMs) for the 2070–2100 SRES A2 emissions scenario. Assuming no further land-use changes these projections will be used together with learning models in further work to predict discharge quantities based on future climate scenarios derived within AT.

2. Study site and data selection

The Gallego river is a tributary of the Ebro river which constitutes the southernmost of five European river basins studied within AT (e.g. Gerzabek et al., in press).

The Gallego originates in the central range of the Pyrenees at the Canal Roya pass and reaches a maximum elevation of 2014 m. The selected gauging point to be modelled is some 100 km further downstream at Anzanigo (580 m). Within this mountainous terrain, the Gallego collects water from several smaller tributaries (see Fig. 1, upper diagram) and has a relatively steep profile (mean slope of 5.1%) for the first 30 km. Below the inflexion of Biescas (after ~30 km) the slope drops to a relatively persistent mean of 0.4% (Ollero et al., 2004).

In terms of rainfall–runoff modelling such a setting can be viewed as challenging, since storage effects from winter snowfall and variability of precipitation events due to topographic control may be substantial. An additional difficulty is that the Gallego river cannot be viewed as a natural flow system (Martinez-Gil (University Zaragoza), 2005, personal communication) with reservoirs (irrigation), channels and hydroelectricity plants regulating large parts of the catchment. For the Upper Gallego river, five reservoirs have been identified as potentially influencing factors: Lanuza, Bubal, Sabinianigo, Jabarella, Javierrelatre (see Table 1 for details).

The Confederacion Hidrografica del Ebro (CHE) holds a large amount of discharge, precipitation, and temperature data available for download at its website: www.chebro.es. These series have multiple start and end dates and some missing data. Missing data for the 01.01.1950 to 30.04.1992 time period were infilled using a day-by-day inverse distance squared interpolation for precipitation data (correlation with elevation on a daily basis appears not as important as for longer time scales, e.g. Ahrens, 2006). Due to the large spatial persistence of temperature series, missing values were obtained from existing temperature data via a day-by-day linear elevation–temperature regression. The precipitation and temperature stations within the Upper Gallego used in the modelling are shown in Fig. 1, upper diagram.

Additionally, daily reservoir volumes at Lanuza and Bubal were also kindly provided by M. Garcia-Vera of the CHE. However, the remaining reservoirs, Sabinianigo, Javierrelatre, and Jabarella, are ungauged. This could represent a considerable source of noise for the rainfall–runoff simulations. Yet, as the capacity of these reservoirs is comparatively small, their influence on daily peak flow estimation is believed to be relatively low. For the simulation of the catchment in its current state, data post 1978 (completion of reservoir Lanuza) were selected. In Fig. 2, the annual total and mean discharge of the Gallego at Anzanigo are given for hydrologic years (October–September) 1979/80 to 1991/92 in a bar chart. This shows that the Gallego catchment underwent a relatively wet phase from 1981 to 1987. Hence, these years were selected for a first model development focussing on peak flow prediction. Since the Lanuza reservoir has no direct influence (buffering through reservoir Bubal) only the Bubal reservoir volume series were included in this study. Furthermore, only precipitation (P) and temperature (T) series downstream of the Bubal reservoir (see Fig. 1, upper diagram) were used. An overview of selected P and T series, as well as reservoir volumes at Bubal (Vol) and discharge (Q) at Anzanigo is given in Fig. 2. The lead time for Q forecasting was set to one day.

Climate change scenarios are constructed using regional climate model data from the EU-Project PRUDENCE. The grid cells used to represent the Gallego catchment and the larger Ebro river basin are shown in Fig. 1, lower diagram.

RCM data from PRUDENCE provide a series of high-resolution regional climate change scenarios for a large range of climatic variables for Europe for the period 2071–2100 using four global climate models (GCMs) and eight RCMs. The construction of climate changes scenarios using a range of models enables an evaluation of the uncertainty of future predictions. For the European domain, individual RCMs provide a greater range of temperature change than the difference between GCMs and RCMs (Déqué et al.,

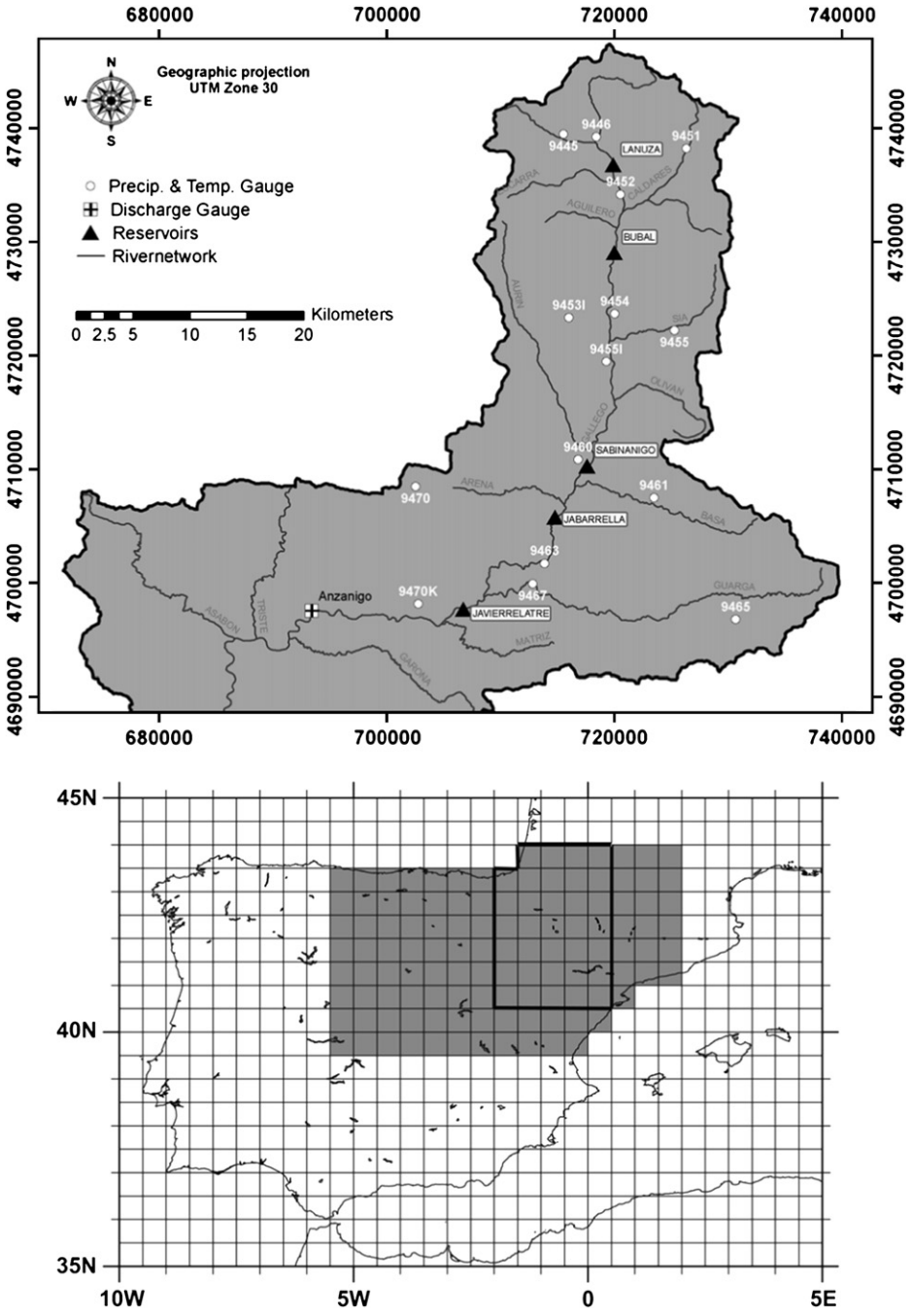

Fig. 1. Upper diagram: map of the Upper Gallego catchment showing gauging station locations, river network and man-made reservoirs. Lower diagram: grid cells used to calculate climate statistics for the Ebro (entire shaded area − 118 cells) and Gallego (boxed subset − 34 cells) catchments.

in press), and inadequate representation of precipitation across Europe. A list of models used in this study and their acronyms is provided in Table 2. Model simulations are available for a control (1961–1990) and future time-slice (2071–2100) for the SRES A2 scenario.

A gridded global series of observed monthly climate means for the period 1901–2000 (Mitchell et al., 2004), CRU TS 2.0 (hereafter referred to as CRU), was used to provide a comparative data set to the RCM control time-slices. Each simulation and the observations were re-gridded onto a common 0.5° by 0.5° grid to allow direct comparison.

Mean monthly climate statistics were calculated for temperature and precipitation at regional and grid-cell scales for both the Ebro and the Gallego catchments to allow model assessment at the impact scale.

3. Learning machines

The theory behind both learning machines applied in this study (i.e. SVM and RVM) is quite involved mathematically and cannot be stated herein detail (for more detail see e.g. Vapnik, 1998 (SVM); Tipping, 2001 (RVM); Schölkopf and

Table 1
Main catchment controlling reservoirs at the Upper Gallego (data kindly provided by M. Garcia-Vera from the CHE)

Reservoir name	Capacity (used/total) (hm^3)	Year of completion
Lanuza	15.00/25.00	1978
Bubal	63.00/64.26	1971
Sabinianigo	0.35/0.41	1965
Jabarella	0.13/0.18	1961
Javierrelatre	0.90/1.16	1966

Smola, 2002 (SVM, RVM)). However, we derive an introductory picture in the following text.

The overall problem of learning from data samples is that their number is finite and that an infinite number of functions exists that could perfectly fit the data according to some error measure (e.g. the root mean squared error (RMSE) is used in this study). If all data samples are used for fitting, there is no way to decide, which function really represents the underlying functional behaviour in the data. Hence, one may pick a function with little predictive ability for an evaluation point that lies between fitted data points. Furthermore, the data may contain noise, and functions fitting the noise (overfitting) are not desired. As a remedy, the data are usually split into a training and test set. The training data are used to derive a trained learning machine, i.e. a fully defined function, whereas the test data are exclusively used to compare the performance of different trained machines on formerly unseen data samples.

Learning machines, in general, can be understood as a set of functions combined with a principle to select one function; that which best approximates the underlying functional behaviour in the training data. Such principles typically try to quantify the trade-off between the 'smoothness' of a function (e.g. similarity to a straight line) and the accuracy of its data fit.

Support vector machines (SVM) and relevance vector machines (RVM) choose functions that are linear in their parameters. More specifically, the functional relationship between an input vector $\mathbf{x}$ (in this study P, T, etc.) and the corresponding outcome y (in this study discharge Q) is approximated by a linear weighting of the outcome of some, possibly non-linear, pre-processing functions K_i (vector and matrix quantities are denoted by bold letters):

$$y \approx f(\mathbf{x}) = \sum_{i=1}^{N} \lambda_i K_i(\mathbf{x}) + \lambda_0 \tag{1}$$

where λ_i with $i = 0,1,\ldots N$ are the corresponding weights and N is the number of pre-processing functions, which corresponds here to the number of training data samples $\{(\mathbf{x}_i,y_i)\}_{i=1}^{N}$.

In the case of the SVM, the K_i are so-called kernel functions or kernels, which satisfy some special mathematical conditions (e.g. Mercer's condition, Mercer, 1909). However, in the case of the RVM, in principle, any set of basis functions (including kernels) could be used. The essential idea is that pre-processing by K_i transforms the data input vector $\mathbf{x}$ into a higher dimensional space, where a linear approximation of the underlying (non-linear) functional relationship is feasible and reasonably accurate. Hence, the choice of kernel is important for learning machine performance in a particular application.

Typical kernel functions are listed in Table 3. In this study preliminary testing suggested radial basis function (rbf) kernels were best for model development. This finding is in accordance with Dibike et al. (2001), who report the best RMSE performance for rbf kernels in the majority of their SVM rainfall–runoff applications.

Despite their similar mathematical formulation (Eq. (1)), learning machines differ substantially in their underlying learning principle (i.e. calculating λ_i and determining the K_i): SVM are based on the statistical learning theory (STL, Vapnik, 1998) and perform structural risk minimization. This can be viewed as ordering different sets of functions by their Vapnik–Chervonenkis dimension (VC, Vapnik and Chervonenkis, 1974) – a measure of the flexibility of a set of functions to fit a functional relationship defined by a finite sample of data. According to STL, the optimal solution can be found by a balanced minimization of both the training error (a property of a particular function f_a) and the VC dimension (a property of the set of functions containing f_a). The balancing and the consideration of noise in this context leads to the introduction of two so-called hyperparameters, C and ε, which are sufficient to compute a trained SVM for a particular kernel. The parameter ε represents an insensitivity to deviations of the prediction function to a training data value up to ε. The hyperparameter C allows for an additional filtering of outlier values. It follows from the SVM formulation that the number of kernel functions used by the SVM may be significantly lower than the number of training data. This results in a so-called 'sparse representation' of the training data set. The remaining data vectors are the name giving 'support vectors'. Suitable values for these hyperparameters, however, have to be obtained by an additional validation procedure. The exact mathematical formulation of the training procedure is beyond the scope of this article. For details see e.g. Vapnik (1998) or Schölkopf and Smola (2002).

In contrast to SVM, the RVM utilizes Bayesian learning (e.g. Berger, 1985). The RVM estimates a normal distribution for y, with the mean of this normal distribution being the most likely value for y. This also includes the uncertainty of the estimate based on the training data set. More formally, Eq. (1) is stated as:

$$y = f(\mathbf{x}) + \delta, \text{ with } \delta \sim N(0,\sigma^2) \tag{2}$$

where δ represents a normally distributed error with zero mean and variance σ^2. The (conditional) distribution over all $\mathbf{y}$ is then:

$$p(\mathbf{y}|\boldsymbol{\lambda},\sigma^2) = (2\pi\sigma^2)^{-N/2}\exp\left(-\frac{1}{2\sigma^2}\|\mathbf{y}-\boldsymbol{\Phi}\boldsymbol{\lambda}\|^2\right) \tag{3}$$

where $\boldsymbol{\lambda} = [\lambda_0,\lambda_1,\ldots,\lambda_N]^t$ and $\boldsymbol{\Phi}$ is an $N(N+1)$ design matrix with $\boldsymbol{\Phi} = [K_1,K_2,\ldots,K_N]^t$ and $K_i = [1,K_i(\mathbf{x}_1),K_i(\mathbf{x}_2),\ldots,K_i(\mathbf{x}_N)]$ (^{t} denotes transpose). Overfitting is avoided in this context by defining explicit prior distributions over the weights $\boldsymbol{\lambda}$:

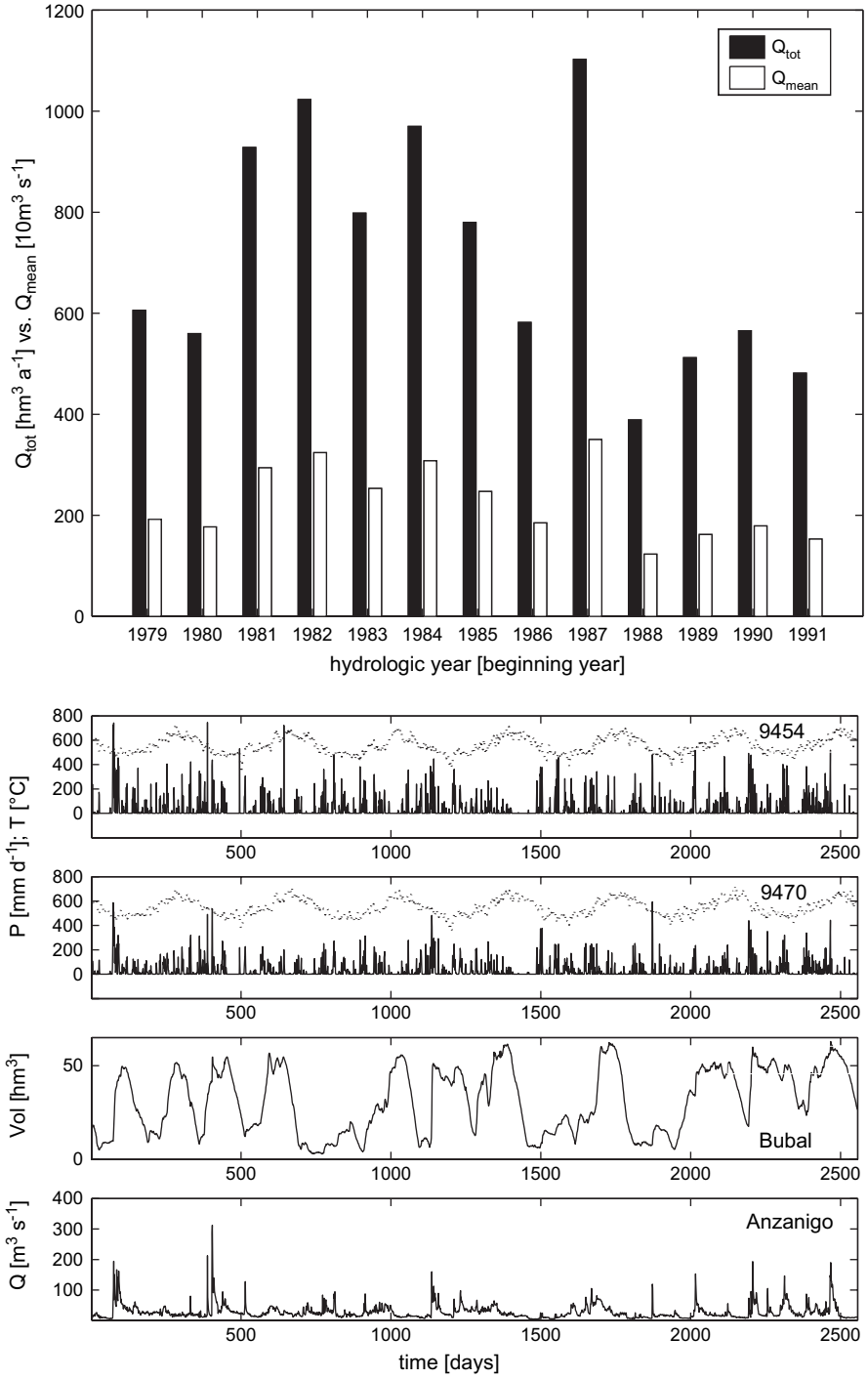

Fig. 2. Upper diagram: annual total discharge and annual mean discharge at Gallego gauging station Anzanigo. Lower diagram: Data series for the selected study period from 1981/82 to 1987/88. Temperature values (T) are stippled, whereas precipitation (P), reservoir volumes (Vol) and discharge (Q) are drawn as solid lines. Please note the temperature series have been shifted by 450 °C for better visualization.

$$p(\boldsymbol{\lambda}|\boldsymbol{\alpha}) = \prod_{i=0}^{N} N\left(\lambda_i \middle| 0, \alpha_i^{-1}\right) \tag{4}$$

with $\boldsymbol{\alpha}$ being a vector of $N+1$ hyperparameters. Using these zero mean, normally distributed prior distributions for the λ_i weights, a preference of smaller weights and, hence, less complex functions is expressed. In fact, during the training procedure it is frequently found that many weights approach zero, which also results in a sparse representation of the data set by the estimated function. The data vectors associated with non-zero weights are called 'relevance vectors' accordingly. As with the SVM the actual training procedure, comprising here the determination of the additional hyperparameters $\boldsymbol{\alpha}$ and the error variance σ^2, is beyond the scope of this article (see Tipping, 2001, 2004 for details).

Table 2
The 11 Regional Climate Models used for this study

	RCM	Driving data	PRUDENCE acronym	AquaTerra acronym
Danish Meteorological Institute (DMI)	HIRHAM	HadAM3H A2	HC1 HS1	HIRHAM_H HIRHAM_H_A2
		ECHAM4/OPYC (OGCM SSTs) A2	Ecctrl ecscA2	HIRHAM_E HIRHAM_E_A2
Swedish Meteorological and Hydrological Institute (SMHI)	RCAO	HadAM3H A2	HCCTL HCA2	RCAO_H RCAO_H_A2
		ECHAM4/OPYC A2	MPICTL MPIA2	RCAO_E RCAO_E_A2
Hadley Centre – UK Met Office	HadRM3P	HadAM3P A2	Adeha adhfa	HAD_P HAD_P_A2
Météo-France, France	Arpège	HadCM3 A2	DA9 DE6	ARPEGE_C ARPEGE_P_A2
The Royal Netherlands Meteorological Institute, Netherlands (KNMI)	RACMO	HadAM3H A2	Control Scenario	RACMO_H RACMO_H_A2
GKSS Forschungszentrum Geesthacht GmbH, Germany (GKSS)	CLM	HadAM3H A2	CTL SA2	CLM_H CLM_H_A2
Swiss Federal Institute of Technology, Switzerland (ETH)	CHRM	HadAM3H A2	HC_CTL HC_A2	CHRM_H CHRM_H_A2
Max Planck Institute for Meteorology, Germany (MPI)	REMO	HadAM3H A2	Control Scenario	REMO_H REMO_H_A2
Universidad Complutense de Madrid, Spain (UCM)	PROMES	HadAM3H A2	Ref A2	PROMES_H PROMES_H_A2

The AquaTerra acronyms are adopted here to provide an easier understanding of the format of each model run. The first part of each acronym refers to the RCM and the second to the GCM data used to provide the boundary conditions. Scenario simulations have the further suffix A2.

The advantage of the presented learning machines is that once the kernel (i.e. the kernel function and its parameter, see Table 3) and hyperparameters (SVM: C and ε, RVM: no undefined hyperparameters) are chosen, there exists a unique training solution. This means that SVM and RVM do not optimise on local minima, as has been noted for ANNs like the multi-layer perceptron (MLP) (e.g. Haykin, 1999). Moreover, the topology selection (e.g. number of hidden neurons in MLP) is reduced to the hyperparameter selection through a validation procedure such as split-sample, k-fold cross-validation (e.g. Haykin, 1999) or bootstrapping (Efron and Tibshirani, 1997). Recent work exploring a variety of such methods in the field of hydro(geo)logy comprises, for example, Anctil and Lauzon (2004) (ANN) and Khalil et al. (2005, 2006) (ANN,SVM, RVM). In this study we minimize the fivefold cross-validation error (RMSE) on the training set to obtain hyper- and kernel parameters. The minimisation for the three SVM parameters was carried out using an evolutionary algorithm for real-valued (global) optimization (see Hansen and Ostermeier, 2001; Hansen et al., 2003; Hansen and Kern, 2004 for details). The single parameter tuning for the RVM was carried out by a bisection algorithm. The MATLAB toolbox The Spider (http://www.kyb.tuebingen.mpg.de/bs/people/spider/) was used for learning machine training and testing.

Table 3
Typical kernel functions ($\mathbf{x}_i$ is a fixed (data) vector)

Formula	Kernel $K_i(\mathbf{x})$
$K_i(\mathbf{x}) = [(\mathbf{x}\cdot\mathbf{x}_i) + 1]^d$	Polynomial kernel of order d (d user defined)[a]
$K_i(\mathbf{x}) = \exp(-\sigma\lvert\mathbf{x} - \mathbf{x}_i\rvert^2)$	Radial basis function kernel (σ user defined)
$K_i(\mathbf{x}) = \tanh(b(\mathbf{x}\cdot\mathbf{x}_i) - c)$	Hyperbolic tangent kernel (b and c user defined)

[a] The · denotes the regular scalar product between two vectors (used in polynomial and hyperbolic tangent kernels).

4. Learning machine development

4.1. Input variables

Input variable selection is an essential task in data-based modelling. As already stated above, a lead time of 1 day is assumed as the mountainous terrain indicates a relatively fast response time and the time discretization sets a minimum lead time of 1 day. Nevertheless, a linear correlation analysis was performed to estimate the delay time between rainfall and the discharge response (see Fig. 3).

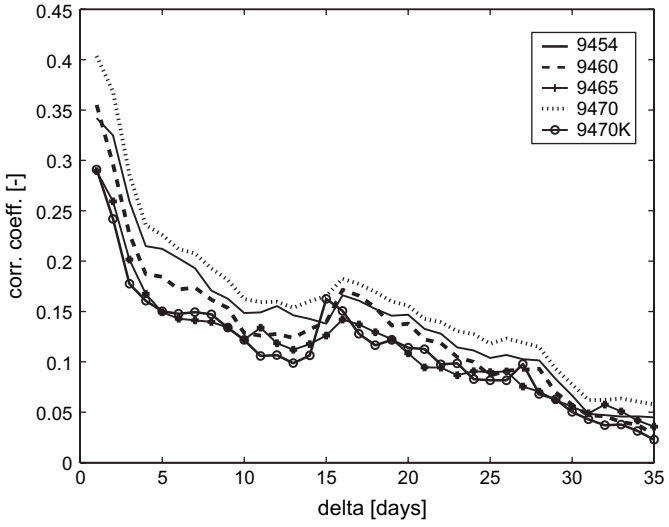

Fig. 3. Linear correlation coefficients between precipitation series (station codes on legend) and shifted (by delta days) discharge series at Anzanigo.

This analysis indicates that a 1-day lead time may correspond to the catchment response time. The relatively steep decline towards a delta of 4 days was interpreted as an indication that individual discharge events can be approximately treated by a short term memory of 4 days per individual precipitation series. Furthermore, the peaking around a delta of 16 days was interpreted as a longer term memory effect. It was therefore decided to include moving window averages of precipitation series within the model. This need is also supported by the fact that during summer months there can be >25 days without rainfall. If only short term rainfall input is considered, this could lead to several zero input vectors (apart from reservoir information) with differing discharge values. For individual learning set-ups, different moving average window sizes, w were used. More precisely, an input vector $\mathbf{x}(t)$ for day t contains the following values of a single precipitation series in order to estimate $Q(t+1)$:

$$\mathbf{x}(t) = \left[\ldots, P(t), P(t-1), P(t-2), P(t-3), \frac{1}{w}\sum_{i=1}^{w} P(t-(3+i)), \ldots\right]$$

where w takes the values 15, 20, 25, and 40. The latter was included to be well above the maximum dry day period. In total, data from 11 precipitation stations were used along with their corresponding daily and moving average temperature values.

Following the reasoning that the daily difference in reservoir volumes should represent the most valuable information for the anthropogenic influence on Gallego discharge, the Vol series was also included with a memory length of 2 days, i.e. Vol(t) and Vol($t-1$) are used to predict $Q(t+1)$.

In this set-up, the catchment state is represented by the long and short term memory of the precipitation series in combination with temperature as, for example, used by Zealand et al. (1999) or Tokar and Markus (2000). The use of future climate change scenarios in the developed learning machine models more or less constrains the input parameters to precipitation and temperature (reservoir operation scenarios could be generated accordingly). Nevertheless, some additional analysis was carried out also using previous discharge values ($Q(t)$ to predict $Q(t+1)$) as e.g. Minns and Hall (1996), Campolo et al. (1999), Anctil and Rat (2005), and de Vos and Rientjes (2005).

4.2. Model set-up

Considering the wet phase of the Gallego between 1981 and 1987, the first 6 years were used for training and the last year for testing. As shown in Fig. 2, the hydrologic year of 1987-1988 shows the largest total annual discharge of the whole data set and may be regarded as a hard test case. However, the highest daily peak flows were reached during 1982-1983 (see Fig. 2 lower diagram), so there should be sufficient information on rainfall–runoff behaviour within the training set.

5. Results

The model development was carried out by the minimization of fivefold cross-validation using RMSE. However, a number of additional performance measures are also presented. The mean absolute error (MAE) is a measure of the absolute accuracy of the model; the index of agreement (IoA, Willmott et al., 1985) and coefficient of efficiency (CoE, Nash and Sutcliffe, 1970) are used due to their sensitivity to additive or proportional differences between model predictions and observations. The IoA ranges from 0.0 to 1.0, where a value closer to one indicates better performance. The CoE ranges from $-\infty$ to 1.0; 1.0 indicates perfect model fit, but at zero model predictions are only as good as the mean over the observations (see e.g. Legates and McCabe, 1999 for a discussion on the use of IoA and CoE in hydrologic model validation). Additionally, the persistence index (PI, Kitanidis and Bras, 1983) is used to compare model performance against a simple model using the discharge value of the previous day as the prediction value for the current day. A PI greater than zero indicates a better performance than simply using the value from the previous day. Formulas for the performance measures are given in the Appendix.

Table 4 shows the performance measures for the learning machine models under consideration. The RVM appears to have higher predictive power on the test set than the SVM, as can be seen from the performance measures.

Table 4
Performance measures values obtained on training and test sets with P, T, Vol input data

Machine type	Performance measure	$w=15$		$w=20$		$w=25$		$w=40$	
		Train	Test	Train	Test	Train	Test	Train	Test
SVM	MAE	6.075	12.846	5.927	12.696	3.667	15.448	4.431	12.806
	RMSE	10.267	20.270	10.149	19.828	7.1402	22.513	8.103	19.751
	IoA	0.930	0.821	0.931	0.832	0.970	0.819	0.960	0.822
	CoE	0.779	0.548	0.784	0.568	0.893	0.443	0.862	0.571
	PI	0.356	−0.623	0.371	−0.556	0.689	−1.011	0.599	−0.545
RVM	MAE	7.730	12.119	7.462	11.881	7.372	11.432	7.588	12.560
	RMSE	10.387	18.823	10.173	18.293	9.995	17.806	10.255	19.388
	IoA	0.932	0.862	0.9353	0.870	0.938	0.876	0.934	0.831
	CoE	0.774	0.611	0.783	0.632	0.791	0.652	0.780	0.587
	PI	0.341	−0.388	0.368	−0.315	0.390	−0.249	0.358	−0.471

Table 5
Performance measures on training and test sets with previous discharge values included

Machine type	Performance measure	$w = 25 + Q(t)$		$w = 40 + Q(t)$		$w = 25 + Q_{ave}$		$w = 40 + Q_{ave}$	
		Train	Test	Train	Test	Train	Test	Train	Test
SVM	MAE			2.646	5.842			2.684	8.031
	RMSE			7.290	13.640			6.825	17.081
	IoA			0.969	0.939			0.973	0.895
	CoE			0.889	0.796			0.902	0.679
	PI			0.675	0.271			0.716	−0.158
RVM	MAE	3.442	6.148			5.314	9.115		
	RMSE	5.791	13.099			7.772	16.370		
	IoA	0.981	0.946			0.965	0.901		
	CoE	0.930	0.811			0.874	0.706		
	PI	0.796	0.304			0.631	−0.057		

These suggest that overall model performance is not very satisfactory on Shamseldin's (1997) scale; demanding a CoE above 0.8 for a 'fairly satisfactory' model. For the best set-ups, with regard to CoE, previous discharge values ($Q(t)$) were added to the data set to provide information on antecedent catchment state. Furthermore, an additional set-up with a moving window average of size $w = 4$ over the previous discharge values (Q_{ave}) was also tested. This average is supposed to provide a suitable baseline, whereas peak flows are generated by the short term precipitation and reservoir data. Table 5 presents the results for the best SVM ($w = 40$ for P and T) and RVM ($w = 25$ for P and T) set-ups with additional previous discharge information after a new kernel- and hyperparameter estimation was performed. These values indicate a considerable improvement in terms of the CoE and other performance measures. Fig. 4 shows the predictions of the best model (RVM with $Q(t)$) on training and test data with 95% confidence intervals. Apart from extreme peaks, the measured curves stay well inside the confidence interval.

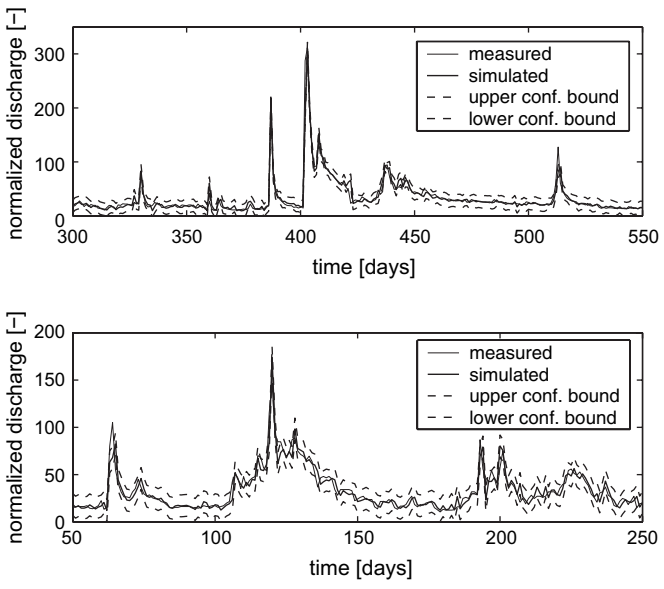

Fig. 4. Best RVM model on training and test data with 95% confidence bounds (previous discharge values used as input data).

6. Climate change projections

6.1. Control climate, 1961–1990

Over the Ebro catchment, all RCMs are skilful in reproducing the annual mean temperature cycle but vary in their ability to reproduce the magnitude of the monthly means (Fig. 5a). RCAO produces the largest overestimates annually (Fig. 5b), with HAD_P producing large positive anomalies during summer. Other models, such as CLM_H, CHRM_H, PROMES_H and ARPEGE_C, underestimate mean temperature in most months. Overall model error is summarised by the mean absolute monthly anomaly (Fig. 5c), indicating that RACMO_H and HIRHAM_H perform best overall, whilst RCAO_E and CLM_H demonstrate the least skill.

The models also vary in their ability to reproduce the spatial distribution of temperature. In particular, during the cooler November–March period, some models have low skill in reproducing observed temperatures over the mountainous northern coast of Spain. For the Gallego there are only small differences in the relative skill of the RCMs compared to the Ebro.

The RCMs reproduce the bimodal distribution of annual precipitation over the Gallego but simulate a large range of values for mean monthly precipitation, particularly from May to August (Fig. 5), suggesting that RCMs differ most in their ability to reproduce summer precipitation processes. This may result from regional climate decoupling from zonal circulation during summer and early autumn when land-sea temperature gradients and topographical influences become more important (Bolle, 2003). RCMs may have more difficulty in representing these meso- to local-scale processes. During these months, several models, which perform with reasonable skill during other periods seemingly fail to capture precipitation processes (Fig. 5). In particular, HIRHAM_H and REMO_H both significantly overestimate mean precipitation by ~60% in July whilst summer precipitation is underestimated by ~50% by RCAO_E and CHRM_H. The mean absolute error suggests that RACMO_H (9.4%) performs best (Fig. 5) whilst CHRM_H is the least skilful (28.8%).

There is little inter-model consistency in the simulation of spatial precipitation patterns. During winter, only the

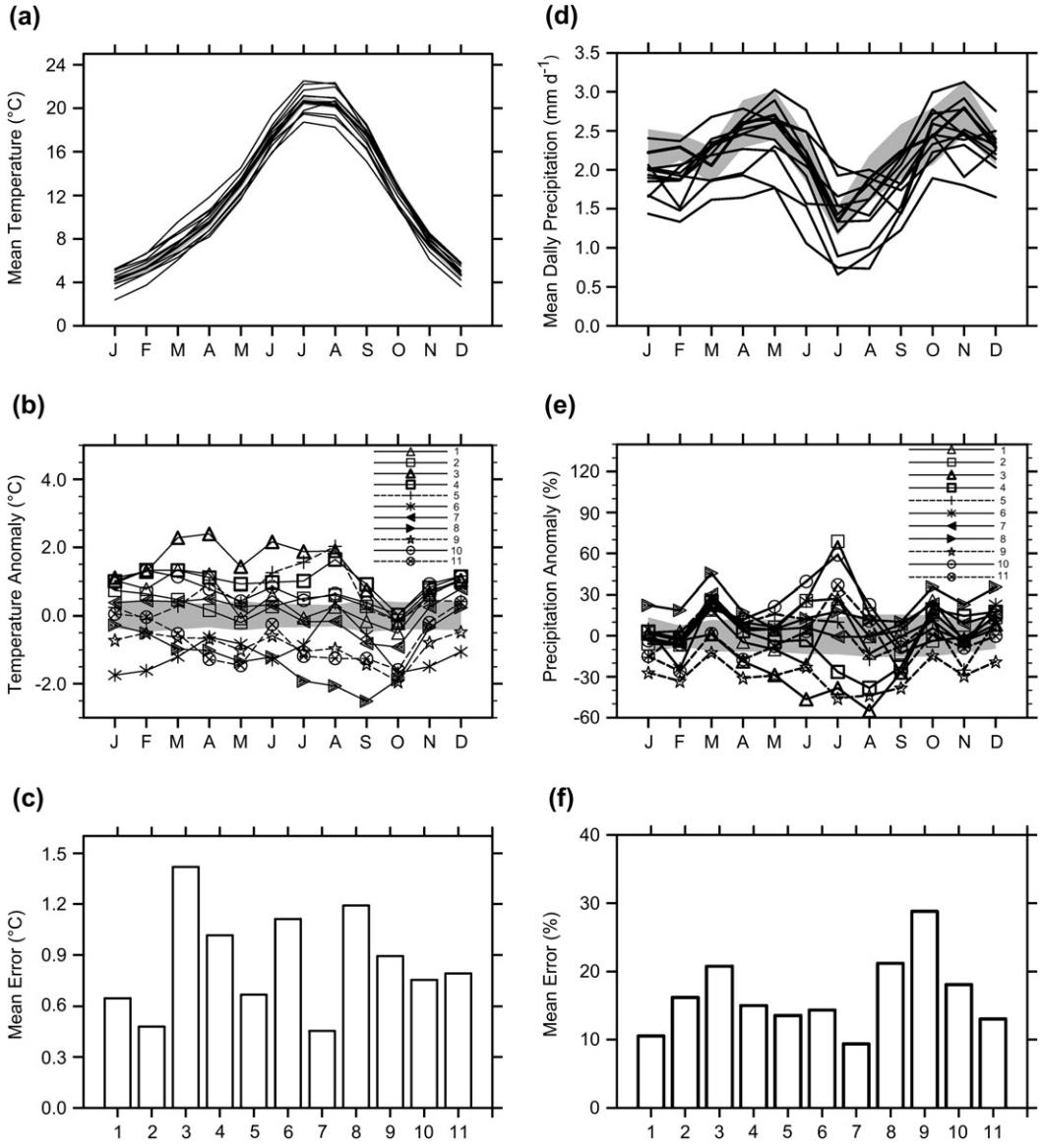

Fig. 5. Left: the mean 1961–1990 monthly temperature for the Ebro catchment. Part (a) shows the annual cycle, each line representing a different RCM simulation and the bold line representing the CRU observed series. The shading represents the 95% confidence interval for the estimate of the observed 30-year sample mean. Part (b) represents the individual monthly model means as an anomaly from the CRU mean with the 95% confidence interval superimposed. Part (c) represents the mean absolute annual error for each of the RCMs. Right: as for left part, but for mean precipitation in the Gallego catchment. Model anomalies in parts (e) and (f) are expressed as a percentage relative to the CRU monthly mean.

HIRHAM and RCAO model pairs produce similar spatial patterns, indicating that the GCM is a less important source of model error than the RCM. This is consistent with Nieto et al. (2004) who indicated that ECHAM4/OPYC3 and HadCM3 both overestimate winter precipitation in the eastern Iberian Peninsula.

6.2. Future scenarios

Under the SRES A2 emissions scenario, temperatures are predicted to increase most in summer months, with smaller rises during winter and early spring. The driving GCM is responsible for the large range of uncertainty in temperature increase (Fig. 6a). ECHAM-driven models project large increases throughout the year. Thus, considerable uncertainty in regional temperature change arises from the different responses of the driving GCMs during summer.

From March to October all RCMs indicate greater warming in the interior of Spain, with lower rates of change along the northern and Mediterranean coast. The magnitude of this increase is greater for ECHAM-driven models. Similar patterns of change are projected for the Gallego catchment, with slightly smaller increases (up to 0.34 °C) between March and July, whilst the unweighted mean of all 11 models produces similar temperature change throughout the year.

For precipitation, the models consistently indicate future decreases (Fig. 6b), although in December and January the models indicate small increases. Most models project the

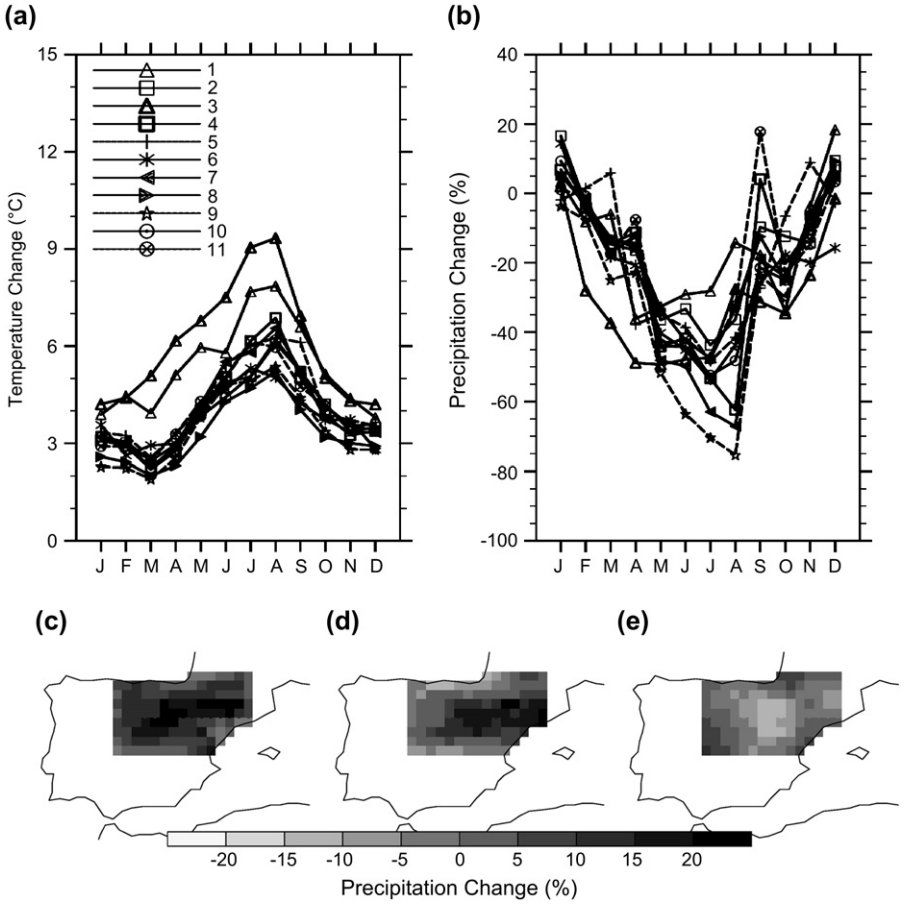

Fig. 6. Projected RCM change in (a) mean temperature and (b) mean precipitation for the Ebro catchment. Change is for 2071–2100 from the 1961–1990 control period and for precipitation is expressed as a percentage of the control mean. Projected change in mean December precipitation for (c) CLM_H, (d) REMO_H for December and (e) RCAO_E.

largest decreases during summer months; up to 75% in August (CHRM_H_A2). When considered together with projected changes in temperature (Fig. 6a), the region is likely to experience milder winters but significantly warmer and drier summers.

The projected increases in December and January precipitation hide variability in the winter distribution of change. The two most commonly projected patterns are: (a) modest increases over the region (Fig. 6c) and (b) decreases over the northern coast and increases over the rest of the region (Fig. 6d). This latter pattern was also obtained for changes in winter precipitation by González-Rouco et al. (2000) using statistically downscaled output from HadCM2. However, there is considerable uncertainty in the spatial distribution of change. In summer, decreases in precipitation are projected but uncertainty surrounds the spatial distribution of change. Several models project increases across the region, whereas others indicate the opposite.

Notwithstanding these uncertainties, the unweighted model means demonstrate that projected changes for the Gallego are similar to those for the larger Ebro catchment (Table 6), with differences between the two regions of $<5\%$ throughout the year.

7. Discussion and conclusions

Learning machine model development based on precipitation, temperature and reservoir information alone provides relatively low model accuracy with respect to the introduced performance measures for both support and relevance vector machines in the Gallego catchment. However, the mountainous topography and the ungauged, but operational, smaller

Table 6
Change in mean monthly precipitation for the Ebro and Gallego catchments

	J	F	M	A	M	J	J	A	S	O	N	D
Ebro	5.3	−5.6	−15.5	−22.2	−41.7	−43.4	−50.5	−43.8	−15.1	−23.0	10.0	4.0
Gallego	2.2	−0.8	−12.0	−18.8	−39.3	−45.1	−51.9	−43.8	−12.8	−21.4	−9.7	4.1

Change is expressed as the mean daily precipitation rate for the period 2071–2100 as a percentage of the 1961–1990 rate.

reservoirs may introduce large amounts of noise into the system that complicate accurate discharge prediction. Furthermore, the time resolution of measurements appears to be close to the catchment response time. In this challenging setting the performance measures indicate that the RVM is a slightly better model than the SVM. The improvement, however, is not substantial for this application.

Additional models were developed using previous discharge values as indirect estimates of antecedent catchment state. The results obtained for both machines were significantly improved; the RVM again achieving the best performance values (Table 5).

de Vos and Rientjes (2005) analysed the use of previous discharge values for runoff prediction using ANNs and concluded that they introduce a strong autoregressive component into the network structure during training. The network is deceived by the high correlation of these inputs with the desired output and filters other important information, such as daily or hourly precipitation values, by assigning them low weights. This, in turn, leads to a peak timing delay of the predicted discharge. This effect is more pronounced for lead times on an hourly scale, but also present in daily forecasts.

Fig. 7 (left and middle diagrams) shows the SVM and RVM model predictions when using previous day discharge as an input parameter. This indicates several places where peaks are delayed or the simulated curve is shifted by one time step compared to the observations, although, major peaks are generally well timed. Predicted discharge sensitivity studies with one percent perturbations of individual input variables showed high sensitivity to previous discharge values, whether low flow, peak flow or randomly picked data samples were perturbed. Although not a detailed theoretical analysis these findings suggest that using previous discharge as input could be problematic for SVM and RVM. However, unlike an ANN, weights in the SVM and RVM formulations used herein do not have direct access to individual components of the input vector.

de Vos and Rientjes (2005) demonstrated taking a moving window average over previous discharge values may improve these peak delays in the ANN case, as the cross-correlation between the moving average and the discharge series is usually lower than the auto-correlation of the latter. Fig. 7 (right diagrams) shows the same parts of the training and test sets, but for RVM simulations based on a moving average set-up. The timing is clearly improved. Yet, the pronounced peak height is again strongly underestimated. Overall, the moving average set-up seems to provide a more realistic estimation, even though it comprises a loss of performance.

Based on the analyses so far, it is concluded that river flow in the Upper Gallego catchment is difficult to simulate with the applied RVM or SVM formulations and the input data types at hand. Nevertheless, a higher time resolution may certainly improve the estimation. A possible future approach could be the combination of learning machines with conceptual model units in order to improve catchment state estimation. Aside from the practical application, a thorough analysis of peak timing delays in the context of learning machines may be worthwhile.

However, for future successful management of water in these types of catchments under climate change, we will increasingly need to develop independent river modelling tools. Climate models suggest that there may be a slight increase in

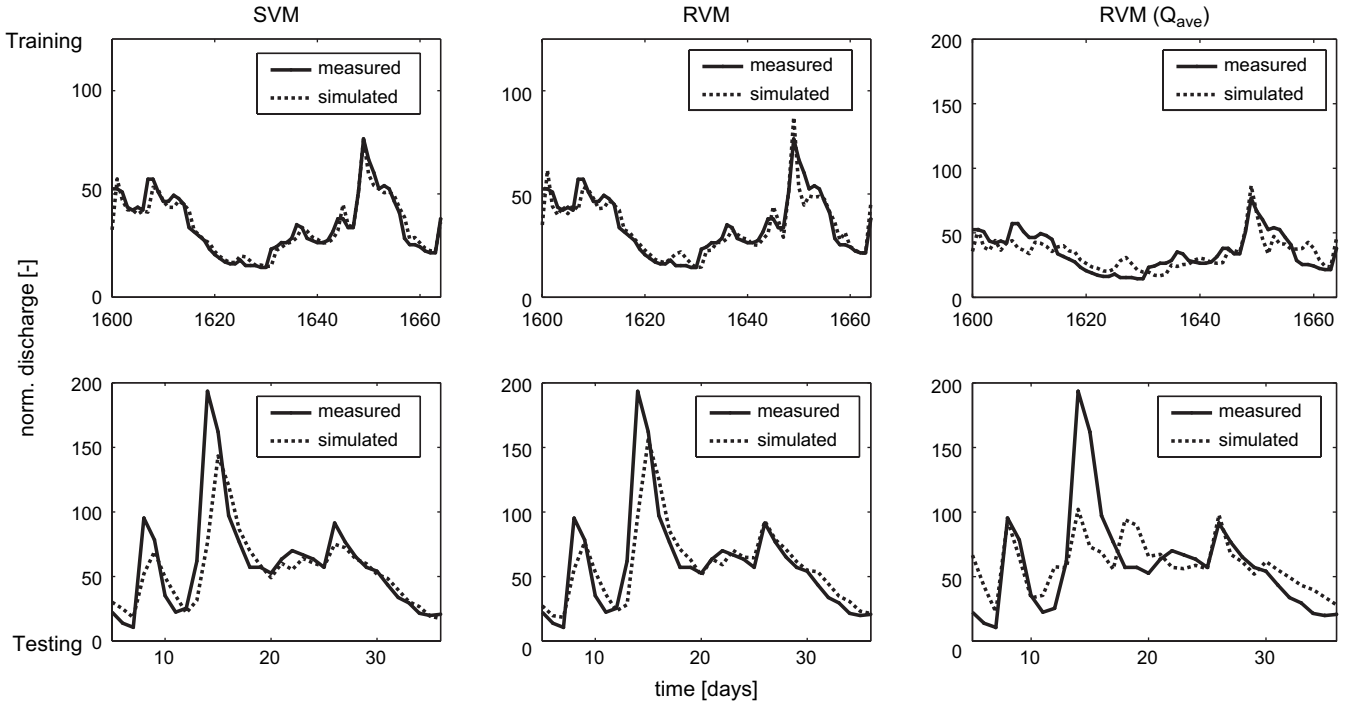

Fig. 7. Close-up of SVM (left) and RVM (middle) predictions on training and test data sets with previous discharge values. Right: close-up of RVM predictions on training and test data sets with moving window average (Q_{ave}) of previous discharge values (window size = 4).

precipitation in the Gallego catchment during winter months but this is more than offset by the large decrease in precipitation projected for the rest of the year. If these projected trends in precipitation are coupled to the projected increases in temperature throughout the year, increasing potential evapotranspiration rates and thus further reducing water availability, it is likely that water supply problems in the Gallego and Ebro catchments may increase. We may therefore need learning machines or more complex combinations of models to help water managers plan for the future.

Acknowledgements

This work was supported by the European Union FP6 Integrated Project AquaTerra (Project no. GOCE 505428) under the thematic priority, sustainable development, global change and ecosystems. Data have been provided through the PRUDENCE data archive, funded by the EU through contract EVk2-CT2001-00132. Data are available to download from http://prudence.dmi.dk/. CRU data set TS 2.0 was made available by Dr. David Viner of the Climatic Research Unit, University of East Anglia. We would like to thank Mr. Miguel Angel Garcia-Vera of the Confederacion Hidrografica del Ebro for his interest and active support of this work. Dr. Jens Hartmann from the Technical University of Darmstadt is also acknowledged for providing contacts and information regarding the Ebro basin. Furthermore, we would like to thank David Kuntz for his highly appreciated map work concerning Fig. 1, upper diagram.

Appendix

In the following O denotes the observed discharge values and P denotes the predicted ones over a data set of n values in timely order. O_{m} denotes the mean of the observed data values.

$$\mathrm{MAE} = \frac{1}{n}\sum_{i=1}^{n}|O_i - P_i|$$

$$\mathrm{RMSE} = \sqrt{\frac{1}{n}\sum_{i=1}^{n}(O_i - P_i)^2}$$

$$\mathrm{IoA} = 1.0 - \frac{\sum_{i=1}^{n}(O_i - P_i)^2}{\sum_{i=1}^{n}(|P_i - O_m| + |O_i - O_m|)^2}$$

$$\mathrm{CoE} = 1.0 - \frac{\sum_{i=1}^{n}(O_i - P_i)^2}{\sum_{i=1}^{n}(O_i - O_m)^2}$$

$$\mathrm{PI} = 1.0 - \frac{\sum_{i=2}^{n}(O_i - P_i)^2}{\sum_{i=2}^{n}(O_i - O_{i-1})^2}$$

References

Abbott, M.B., Bathurst, J.C., Cunge, J.A., O'Connell, P.E., Rasmussen, J., 1986. An introduction to the European hydrological system – Systeme Hydrologique Europeen, "SHE". 2: structure of a physically-based, distributed modelling system. Journal of Hydrology 87, 45–59.

Ahrens, B., 2006. Distance in spatial interpolation of daily rain gauge data. Hydrology and Earth System Sciences 10, 197–208.

Anctil, F., Lauzon, N., 2004. Generalization for neural networks through data sampling and training procedures, with applications to streamflow predictions. Hydrology and Earth System Sciences 8 (5), 940–958.

Anctil, F., Rat, A., 2005. Evaluation of neural network streamflow forecasting on 47 watersheds. Journal of Hydrologic Engineering 10 (1), 85–88.

Anctil, F., Michel, C., Perrin, C., Andreassian, V., 2004. A soil moisture index as an auxiliary ANN input for stream flow forecasting. Journal of Hydrology 286, 155–167.

Asefa, T., Kemblowski, M., McKee, M., Khalil, A., 2006. Multi-time scale stream flow predictions: the support vector machines approach. Journal of Hydrology 318, 7–16.

Berger, J.O., 1985. Statistical Decision Theory and Bayesian Analysis, second ed. Springer.

Beven, K.J., Freer, J., 2001. A dynamic TOPMODEL. Hydrological Processes 15 (10), 1993–2011.

Bolle, H.-J., 2003. Climate, climate variability, and impacts in the Mediterranean area: an overview. In: Bolle, H.-J. (Ed.), Mediterranean Climate. Springer, Berlin, p. 372.

Boser, B.E., Guyon, I.M., Vapnik, V.N., 1992. A training algorithm for optimal margin classifiers. In: Haussler, D. (Ed.), Proceedings of the Annual Conference on Computational Learning Theory. ACM Press, Pittsburgh, PA, pp. 144–152.

Campolo, M., Andreussi, P., Soldati, A., 1999. River flood forecasting with a neural network model. Water Resources Research 35 (4), 1191–1197.

Chen, J., Barry, A.J., 2006. Integration of artificial neural networks with conceptual models in rainfall–runoff modeling. Journal of Hydrology 318, 232–249.

Dawson, C.W., Wilby, R.L., 1999. A comparison of artificial neural networks used for river flow forecasting. Hydrology and Earth System Sciences 3 (4), 529–540.

Dawson, C.W., Abrahart, R.J., Shamseldin, A.Y., Wilby, R.L., 2006. Flood estimation at ungauged sites using artificial neural networks. Journal of Hydrology 319, 391–409.

De Luís, M., Raventós, J., González-Hidalgo, J.C., Sánchez, J.R., Cortina, J., 2000. Spatial analysis of rainfall trends in the region of Valencia (East Spain). International Journal of Climatology 20, 1451–1469.

Déqué M., Rowell D., Schär C., Giorgi F., Christensen J.H., Rockel B., Jacob D., Kjellstrom E. De Castro M., and van den Hurk B. An intercomparison of regional climate models for Europe: assessing uncertainties in model projections. Climatic Change, in press.

Dibike, Y.B., Velickov, S., Solomatine, D., Abbott, M.B., 2001. Model induction with support vector machines: introduction and applications. Journal of Computing in Civil Engineering 15 (3), 208–216.

Efron, B., Tibshirani, R.J., 1997. Improvements on cross-validation: the 0.632 + bootstrap method. Journal of The American Statistical Association 92 (438), 548–560.

Esteban-Parra, M.J., Pozo-Vázquez, D., Rodrigo, F.S., Castro-Díez, Y., 2003. Temperature and precipitation variability and trends in Northern Spain in the context of the Iberian Peninsula climate. In: Bolle, H.-J. (Ed.), Mediterranean Climate. Springer, Berlin, p. 372.

Gautam, M.R., Watanabe, K., Saeguse, H., 2000. Runoff analysis in a humid forest catchment with an artificial neural network. Journal of Hydrology 235, 117–136.

Gerzabek, M.H., Barcelo, D.A.B., Rijnaarts, H.H.M., Slob, A., Darmendrail, D., Fowler H.J., Negrel, P., Frank, E., Grathwohl, P., Kuntz, D., Barth, J.A.C. The integrated project aquaterra of the eu sixth framework lays foundations for better understanding of river–sediment–soil–groundwater systems. Journal of Environmental Management, in press. doi:10.1016/j.jenvman.2006.10.014.

González-Rouco, J.F., Heyen, H., Zorita, E., Valero, F., 2000. Agreement between observed rainfall trends and climate change simulations in the Southwest of Europe. Journal of Climate 13, 3057–3065.

Goodess, C.M., Jones, P.D., 2002. Links between circulation and changes in the characteristics of Iberian rainfall. International Journal of Climatology 22, 1593–1615.

Hansen, N., Ostermeier, A., 2001. Completely derandomized self-adaptation in evolution strategies. Evolutionary Computation 9 (2), 159–195.

Hansen, N., Kern, S., 2004. Evaluating the CMA evolution strategy on multimodal test functions. In: Eighth International Conference on Parallel Problem Solving from Nature PPSN VIII, Proceedings. Springer, pp. 282–291.

Hansen, N., Müller, S.D., Koumoutsakos, P., 2003. Reducing the time complexity of the derandomized evolution strategy with covariance matrix adaptation (CMA-ES). Evolutionary Computation 11 (1), 1–18.

Haykin, S., 1999. Neural Networks – A Comprehensive Foundation, second ed. Prentice Hall, Upper Saddle River, New Jersey.

Jain, A., Srinivasulu, S., 2004. Development of effective and efficient rainfall–runoff models using integration of deterministic, real-coded genetic algorithms and artificial neural network techniques. Water Resources Research 40, W04302, doi:10.1029/2003WR002355.

Khalil, A., Almasri, M.N., McKee, M., Kaluarachchi, J.J., 2005. Applicability of statistical learning algorithms in groundwater quality modeling. Water Resources Research 41, W05010, doi:10.1029/2004WR003608.

Khalil, A.F., McKee, M., Kemblowski, M., Asefa, T., Bastidas, L., 2006. Multiobjective analysis of chaotic dynamic systems with sparse learning machines. Advances in Water Resources 29 (1), 72–88.

Kitanidis, P.K., Bras, R.L., 1983. Real-time forecasting with a conceptual hydrologic model. 2. Applications and results. Water Resources Research 16 (6), 1034–1044.

Legates, D.R., McCabe, G.J., 1999. Evaluating the use of ''goodness-of-fit'' measures in hydrologic and hydroclimatic model validation. Water Resources Research 35 (1), 233–241.

Martínez, M.D., Lana, X, Burgueño, A, Serra, C, 2007. Spatial and temporal daily rainfall regime in Catalonia (NE Spain) derived from four precipitation indices, years 1950–2000. International Journal of Climatology 27 (1), 123–138.

Mitchell, T.D., Carter, T.R., Jones, P.D., Hulme, M., New, M., 2004. A comprehensive set of high-resolution grids of monthly climate for Europe and the globe: the observed record (1901–2000) and 16 scenarios. In: Tyndall Working Paper, 55. Tyndall Centre, UEA, Norwich.

Mercer, J., 1909. Functions of positive and negative type and their connection with the theory of integral equations. Philosophical Transactions of the Royal Society of London, A 209, 415–446.

Minns, A.W., Hall, M.J., 1996. Artificial neural networks as rainfall–runoff models. Hydrological Sciences Journal 41, 399–417.

Nash, J.E., Sutcliffe, J.V., 1970. River flow forecasting through conceptual models. I. A discussion of principles. Journal of Hydrology 10, 282–290.

Nieto, S., Frías, M.D., Rodríguez-Puebla, C., 2004. Assessing two different climatic models and the NCEP-NCAR reanalysis data for the description of winter precipitation in the Iberian Peninsula. International Journal of Climatology 24, 361–376.

Ollero, A., Sanchez, M., Marin, J.M., Fernandez, D., Ballarin, D., Mora, D., Montorio, R., Begueria, S., Zuniga, M., 2004. Caracterizacion Hidromorfological del Rio Gallego. In: Pena, J.L., Longares, L.A., Sanchez, M. (Eds.), Geografia Fisica de Aragon. Aspectos generales y tematicos. Universidad de Zaragoza e Institucion Ferndando el Catolico, Zaragoza (Spain), pp. 117–129.

Palutikof, J., 2003. Analysis of Mediterranean climate data: measured and modelled. In: Bolle, H.-J. (Ed.), Mediterranean Climate. Springer, Berlin, pp. 372.

Ramos, M.C., Martínez-Casasnovas, J.A., 2006. Trends in precipitation concentration and extremes in the Mediterranean Penedès-Anoia Region, NE Spain. Climatic Change 74, 457–474.

Rajurkar, M.P., Kothyari, U.C., Chaube, U.C., 2004. Modeling of the daily rainfall–runoff relationship with artificial neural network. Journal of Hydrology 285, 96–113.

Sajikumar, N., Thandaveswara, B.S., 1999. A non-linear rainfall–runoff model using an artificial neural network. Journal of Hydrology 216, 32–55.

Shamseldin, A.Y., 1997. Application of a neural network technique to rainfall–runoff modelling. Journal of Hydrology 199, 272–294.

Sivakumar, B., Jayawardena, A.W., Fernando, T.M.K.G., 2002. River flow forecasting: use of phase–space reconstruction and artificial neural networks approaches. Journal of Hydrology 265, 225–245.

Schölkopf, B., Smola, A., 2002. Learning with kernels: support vector machines, regularization, optimization and beyond. MIT Press, Cambridge, MA, USA.

Tipping, M., 2001. Sparse Bayesian learning and the relevance vector machine. Journal of Machine Learning Research 1, 211–244.

Tipping, M.E., 2004. Bayesian inference: an introduction to principles and practice in machine learning. In: Bousquet, O., von Luxburg, U., Rätsch, G. (Eds.), Advanced Lectures on Machine Learning. Springer, pp. 41–62.

Tokar, A.S., Markus, M., 2000. Precipitation–runoff modeling using artificial neural networks and conceptual models. Journal of Hydrologic Engineering 5 (2), 156–160.

de Vos, N.J., Rientjes, T.H.M., 2005. Constraints of artificial neural networks for rainfall–runoff modelling: trade-offs in hydrological state representation and model evaluation. Hydrology and Earth System Sciences 9, 111–126.

Vapnik, C.N., 1998. Statistical Learning Theory. Wiley, NY, USA.

Vapnik, C.N., Chervonenkis, A., 1974. Theory of Pattern Recognition. Nauka, Moscow (in Russian).

Weiler, M., McGlynn, B.L., McGuire, K.J., McDonnel, J.J., 2003. How does rainfall become runoff? A combined tracer and runoff transfer function approach. Water Resources Research 39 (11), doi:10.1029/2003WR002331.

Willmott, C.J., Ackleson, S.G., Davis, R.E., Feddema, J.J., Klink, K.M., Legates, D.R., O'Donnell, J., Rowe, C.M., 1985. Statistics for the evaluation and comparison of models. Journal of Geophysical Research 90, 8995–9005.

Zealand, C.M., Burn, D.H., Simonovic, S.P., 1999. Short term stream flow forecasting using artificial neural networks. Journal of Hydrology 214, 32–48.